HHS Public Access

Author manuscript

Nat Microbiol. Author manuscript; available in PMC 2019 April 01.

Published in final edited form as:

Nat Microbiol. 2018 December ; 3(12): 1362–1368. doi:10.1038/s41564-018-0255-y.

Structural basis for usher activation and intramolecular subunit transfer in P pilus biogenesis in *E. coli*

Natalie S. Omattage[1,2], **Zengqin Deng**[3,4], **Jerome S. Pinkner**[1,2], **Karen W. Dodson**[1,2], **Fredrik Almqvist**[5,6], **Peng Yuan**[#3,4], and **Scott J. Hultgren**[#1,2]

[1]Department of Molecular Microbiology, Washington University in St Louis, St Louis, Missouri 63110, USA.

[2]Center for Women's Infectious Disease Research (CWIDR), Washington University in St Louis, St Louis, Missouri 63110, USA

[3]Department of Cell Biology and Physiology, Washington University in St Louis, St Louis, Missouri 63110, USA.

[4]Center for the Investigation of Membrane Excitability Diseases, Washington University in St Louis, St Louis, Missouri 63110, USA.

[5]Department of Chemistry, Umeå University, Umeå, Sweden

[6]Umeå Center for Microbial Research, Umeå University, Umeå, Sweden

[#] These authors contributed equally to this work.

Abstract

Chaperone-usher pathway (CUP) pili are extracellular proteinaceous fibers ubiquitously found on Gram-negative bacteria, and mediate host-pathogen interactions and biofilm formation critical in pathogenesis in numerous human diseases[1]. During pilus assembly an outer membrane (OM) macromolecular machine called the usher catalyzes pilus biogenesis from the individual subunits that are delivered as chaperone-subunit complexes in the periplasm. The usher orchestrates pilus assembly using all five functional domains: a 24-stranded transmembrane β-barrel translocation domain (TD), a β-sandwich plug domain (PD), an amino-terminal periplasmic domain (NTD) and two carboxy-terminal periplasmic domains (CTD1 and CTD2)[2–6]. Despite extensive structural and functional characterization, the mechanism by which the usher is activated to initiate pilus biogenesis is unknown. Here we present the crystal structure of the full-length PapC usher from *Escherichia coli* in complex with its cognate PapDG chaperone-subunit complex in a pre-

Corresponding authors: Scott J. Hultgren, Department of Molecular Microbiology, Washington University in St Louis, St Louis, Missouri 63110, USA. (Hultgren@wustl.edu) or Peng Yuan, Department of Cell Biology and Physiology, Washington University in St. Louis, St. Louis, Missouri, 63110, USA. (yuanp@wustl.edu).

Author Contributions

N.S.O. expressed and purified protein, produced and crystallized the PapC-PapDG complex. N.S.O. and Z.D collected X-ray data and determined the structure. P.Y. supervised crystallography work. J.S.P. expressed and purified protein. S.J.H., P.Y, N.S.O., and Z.D. designed and N.S.O. performed *in vitro* functional and biochemical assays. S.J.H., P.Y., K.W.D., F.A., Z.D. and N.S.O. wrote the manuscript with input from all authors.

Competing Interests

The authors declare no competing financial interests.

activation state, elucidating molecular details of how the usher is specifically engaged by allosteric interactions with its substrate preceding activation and how the usher facilitates the transfer of subunits from the NTD to the CTDs during pilus assembly. This work elucidates the intricate workings of a molecular machine that catalyzes CUP pilus assembly and opens the door for the development of potent inhibitors to block pilus biogenesis.

Main

Gram-negative bacteria assemble CUP pili to mediate adhesion to host and environmental surfaces, facilitate invasion into host tissues, and promote formation of intra- and extra-cellular biofilm communities[1]. This has been best studied for urinary tract infections (UTIs), which affect 60% of women in their lifetime[7,8]. *Escherichia coli* (*E. coli*) carries at least 38 CUP pili in its pan genome[9]. Uropathogenic *E. coli* (UPEC), the causative agent of 85% of community-acquired UTIs, utilizes type 1 and P pili to mediate host- and tissue-specific adherence critical in cystitis and pyelonephritis, respectively [10–14].

In CUP pilus assembly, individual pilus subunits or pilins are first exported across the inner membrane to the periplasm where they are guided to the OM usher via the chaperone[15,16]. Each pilin adopts an incomplete immunoglobulin (Ig)-like structure lacking a seventh C-terminal β-strand[17,18]. In a process termed *donor-strand complementation* (DSC), the chaperone, a boomerang shaped protein comprised of two complete Ig-like domains, provides *in trans* its G1 β-strand to complete the pilin's Ig-like fold in a non-canonical fashion[17,18]. Chaperone-pilin complexes are then guided to the OM usher, a β-barrel channel that catalyzes subunit-subunit interactions through a reaction called *donor-strand exchange* (DSE) wherein an N terminal extension on every subunit completes the canonical Ig fold of its neighboring subunit in a zip-in zip-out mechanism that drives the dissociation of the chaperone[19–21].

DSE events are coordinated by the PapC usher and require all five functional domains of the usher for productive interactions between pilus subunits during fiber polymerization[4,22]. In biolayer interferometry (BLI) studies, the isolated NTD binds the chaperone-adhesin PapDG complex with the highest affinity relative to other chaperone-subunit complexes[23]. Thus, P pilus assembly is thought to begin with the recruitment of PapDG to the NTD of apo-PapC. Unlike the NTD, the PD and the PD-NTD complex bind the chaperone and all chaperone-subunit complexes with nearly equal affinity[23]. Based on studies in the type 1 pilus system, chaperone-subunit complexes are transferred from the NTD to the CTD by an unknown mechanism[4,22]. The PapC CTD2 has been shown to promote the dissociation of PapDG from the NTD *in vitro*[23]. In BLI studies, CTD2 binds to all tested chaperone-subunit complexes except the PapDH complex[23]. Incorporation of PapH results in termination of pilus biogenesis[24,25]. Thus, the CTDs are thought to facilitate the hand-off of chaperone-subunit complexes from the NTD to the CTDs by an unknown mechanism, resulting in their association at the usher CTDs during activation of the usher for the initiation of pilus assembly and all subsequent pilus assembly elongation steps[4,22]. We define usher activation as a complex multi-step mechanism, which begins with the interactions between the chaperone-adhesin and usher NTD and results in: i) its association with NTD in the

periplasm; ii) transfer of chaperone-adhesin from the NTD to CTDs and; iii) Plug domain displacement. Here we present an X-ray crystal structure of the ternary PapC-PapDG complex in the process of transitioning from an inactive to a post-activation state, termed here a pre-activation state, delineating detailed molecular interactions between PapDG and the NTD and CTD2 of PapC. Addition of the PapDF chaperone-pilin complex to the pre-activated PapC-PapDG complex results in DSE between PapG and PapF. Mutations in the NTD-CTD2 interface significantly reduced pilus assembly *in vivo* and diminished the ability of PapC to promote PapG-PapF DSE *in vitro*. Together with functional characterization and comparison with the post-activation structures in the type 1 pilus system, our results reveal critical details about the molecular mechanism of usher activation and chaperone-adhesin translocation from the usher NTD to CTD.

The ushers that assemble the most well characterized CUP pili, the type 1 pilus and P pilus, have a sequence identity and similarity of 31% and 43%, respectively, but exhibit high structural similarity and are thought to share common assembly mechanisms. Thus, genetic, biochemical, and biophysical studies conducted in either pilus system are often combined to elucidate the molecular determinants of usher function during pilus biogenesis. However, variations in pilus assembly mechanisms have been noted in different pilus systems. In type 1 pilus biogenesis, the FimH adhesin is sufficient to activate the FimD usher to initiate pilus assembly[26,27]. In marked contrast, in the P pilus system, efficient activation of the PapC usher involves a concerted mechanism involving both the PapG adhesin and the subsequent pilus subunit and adaptor protein, PapF[28–30]. In order to elucidate the mechanism by which PapC is primed for activation and its transition to a post-activation state we: i) reconstituted a ternary PapC-PapDG complex *in vitro* without PapF (**Figs. 1a and 1b**); ii) crystallized the ternary PapC-PapDG complex and; iii) determined the crystal structure at 3.7 Å resolution (**Fig. 1d, Supplementary Table 1**). To demonstrate the activity of the isolated PapC-PapDG complex we used a DSE assay to determine if the usher in the PapC-PapDG complex could promote DSE between PapG and PapF upon addition of the PapDF complex (**Fig. 1c**). Indeed, appearance of an SDS stable PapGF band appeared over time, albeit slowly, signifying that the purified PapC-PapDG ternary complex is capable of promoting DSE *in vitro*. In the time course tested, the DSE reaction between PapG and PapF does not achieve 100% completion, but this is consistent with the reported DSE rate between PapG and PapF (~50% completion in 120 hours)[31,32]. Moreover, the sample at the end of the time course could be purified and was demonstrated to have formed a quaternary PapC-PapDFG complex (**Supplementary Fig. 1**). Though it is likely that the reconstituted PapC-PapDG complex exists as a mixture of pre-activated and post-activated conformations, the crystal structure reveals a pre-activated usher state transitioning to a post-activation state in which: i) the PD still resides within the β-barrel lumen and; ii) the NTD and CTDs interact with each other and both are also engaged in binding PapDG (**Fig. 1d and Fig. 2a-b**). This is in sharp contrast to the previously determined crystal structures of usher-chaperone-adhesin FimD-FimCH, and usher-tip fibrillum, FimD-FimCFGH complexes from the type 1 pilus system, in which the FimD usher has already transitioned to a post-activation state[4,22]. In the FimD-FimCH and FimD-FimCFGH structures: i) the PD of FimD has translocated into a periplasmic NTD-PD complex; ii) the chaperone-subunit complex has been transferred to the CTDs and; iii) the adhesin lectin domain ($FimH_L$) is inserted into the β-barrel pore (**Fig.**

2a). Notably, the FimD-FimCH structure was achieved by limited proteolysis with trypsin prior to crystallization[4], which resulted in cleavage of the N-terminal tail of the FimD usher, a critical motif for binding the chaperone-adhesin complex and subsequent chaperone-subunit complexes[33–35]. Since the critical NTD tail was removed in that study, the NTD-chaperone-adhesin and NTD-CTD2 interactions elucidated in our wild-type PapC-PapDG structure, in which the N-terminal tail of the PapC usher is critically engaged with both the chaperone-adhesin and in the NTD-CTD2 interface, could not be observed. Thus, it also raises the possibility that all (full-length) ushers, when incubated with their cognate chaperone-adhesin complex, remain in a pre-activation state until an additional subunit is recruited to the usher, competing for the N-terminal tail residues to release the chaperone-adhesin from the NTD to undergo complete translocation to the CTDs and enter the TD lumen (**Supplementary Fig. 2a**).

In the PapC-PapDG structure, both the NTD and CTD2 are in substantially different positions as compared with the previous type 1 pilus post-activation structures (**Fig. 2c-d**). These large domain rearrangements are made possible by flexible linkers connecting the NTD to the TD and CTD2 to CTD1. CTD1 remains stationary between the pre-activation and post-activation states, suggesting that CTD2 is the dynamic component of the bi-partite CTD of the usher. The PapDG complex in our structure has an essentially identical structure to isolated PapDG (**Supplementary Fig. 3**). The adhesin lectin domain ($PapG_L$) resides at the base of the β-barrel, burying ~490 $Å^2$ of surface area, and does not interact with any periplasmic domains of the usher (**Fig. 2e**). The adhesin pilin domain ($PapG_P$) moves along the same rotational axis as CTD2 (**Fig. 2e**). The initial binding of the PapC usher NTD and the PapDG chaperone-adhesin complex does not immediately elicit the PD displacement that primes the β-barrel for pilus extrusion through the pore. Conceptually, the PD displacement may occur concurrently with recruitment of the subsequent chaperone-subunit complex, PapDF, to the NTD and translocation of PapDG to the CTDs (**Supplementary Fig. 2a**). Alternatively, complete translocation of PapDG to the CTDs might elicit PD displacement followed by recruitment of PapDF to an NTD-PD complex (**Supplementary Fig. 2b**).

While the PD resides within the pore lumen, the periplasmic domains make extensive contacts with PapDG as well as with each other, giving rise to a pre-activated usher in the process of activation. The PapC NTD interacts, via the first eleven amino acids of its N-terminal tail, with PapD (**Fig. 3a**). In particular, the conserved F3 of PapC plugs into a hydrophobic pocket comprised of residues P30, L32, I93, and P95 of PapD (**Fig. 3a**). Mutation of F3 of the usher or L32 and I93 of the chaperone abolishes pilus assembly, suggesting that this interface is critical in usher function[3,35]. Additionally, the usher CTD2 also contacts PapD, with D762 of CTD2 forming a salt bridge with K44 of PapD, an interaction also observed in the FimD-FimCH and FimD-FimCFGH structures (**Fig. 3b**)[4,22].

Remarkably, direct intra-usher interactions between the usher NTD and CTD2 are also observed at the NTD-PapDG-CTD2 interface (**Fig. 3c**). Despite the medium resolution of the structure, the N-terminal tail residues 12–21 of the NTD are well resolved in the electron density map (**Supplementary Fig. 4**) and form extensive interactions with the bottom cleft of CTD2, particularly the β1-β2 and β5-β6 loops in CTD2 (**Fig. 3c**). While the interactions

between CTD2 and the chaperone are observed in the post-activation FimD-FimCH structure (**Supplementary Fig. 5**), the NTD-CTD2 interface is an unprecedented, unique feature in our pre-activation PapC-PapDG structure. This interface was not observed in the FimD-FimCH structure because the NTD motif was proteolytically removed by trypsin to aid in crystallization[6]. To evaluate the physiological relevance of this NTD-CTD2 interface, we made multiple mutations in amino acids comprising this interface, with a focus on an N-terminal α-helix in the usher NTD that is positioned directly next to CTD2 (**Fig. 3c**)[3,33]. To investigate their functional importance, we tested the ability of each PapC mutant to complement a Δ*papC pap* operon (*papAHDJKEFG*) in a hemagglutination assay, which is a measure of overall levels of piliation on the bacterial surface (HA titer analysis) (**Fig. 3d**). All mutations in this region, especially mutants destabilizing the α-helix, resulted in a significant reduction in HA titer, ranging from a complete ablation of HA titer to a 2- to 16-fold decrease in HA titer (**Fig. 3d**). These defects in P pilus assembly are specific to this interface as mutations of surrounding residues on the N-terminal tail or CTD2 have no effect (**Supplementary Fig. 6**).

To further interrogate the role of this interface in usher activation, we selected four PapC mutants (D17P, (16–20)A, F21A, and F745A) and tested their ability to first form a stable ternary complex with PapDG and then to promote DSE between PapG and PapF (**Fig. 4**). Mutations destabilizing the N-terminal α-helix (D17P or (16–20)A) or a residue flanking the end of the α-helix (F21A) resulted in an inability of the mutant PapC ushers to form a stable ternary complex *in vitro* (**Fig. 4a-c**). Interestingly, the F21A PapC mutant had been previously characterized as exhibiting an HA titer defect and reduced association with PapDG, and was proposed to be involved in subunit discrimination during pilus assembly[28]. In light of our structure, it appears that this residue may play a role in stabilizing an NTD-CTD2 interface during a pre-activation usher state. Contrary to the NTD mutants, the CTD2 mutant (F745A) retained its ability to form a stable ternary complex with PapDG *in vitro* but was not able to efficiently promote DSE between PapG and PapF relative to wild-type PapC-PapDG (**Fig. 4d-f**). Taken together, these results demonstrate that the NTD-CTD2 interaction is essential for stable association of PapDG with the PapC usher and translocation of subunits from the NTD to CTDs, further suggesting that our wild-type PapC-PapDG structure represents a productive on-pathway intermediate rather than an off-pathway conformation owing to detergent solubilization and crystallization, although additional studies will be required to address this possibility. Moreover, our structure-function analysis of PapC-PapDG suggests that CTD2 drives subunit transfer, potentially by using the avidity of its interactions with both the NTD and PapD to competitively displace subunits from the NTD during pilus biogenesis (**Fig. 3e**). Several lines of evidence further support this competitive displacement mechanism. First, previous BLI studies have shown that in isolation CTD2 can promote dissociation of a chaperone-adhesin bound to the NTD[23]. Second, it has been shown in the type 1 pilus system that upon usher activation the CTDs are the high affinity binding site (K_d = 40 nM) in the full-length usher compared to the NTD (K_d = 389 nM)[36]. Therefore, these data suggest this differential affinity potentially drives translocation from the NTD to the CTDs, and our structure further demonstrates allosteric destabilization of the chaperone-subunits at the NTD may be facilitated by a direct interaction between the NTD and CTD2.

The chaperone-usher pathway represents an ideal system in which to study the mechanisms by which binding and allosteric interactions drive sequential steps in a multi-domain assembly machine without ATP or other energy inputs. This work provides insight into the mechanism by which the outer membrane usher transfers substrates from its N-terminus to C-terminus via an unexpected interaction between two periplasmic domains. Previously, bicyclic 2-pyridone compounds termed pilicides were determined to be inhibitors of pilus biogenesis by specifically blocking chaperone-subunit interactions with the N-terminal tail of the usher NTD[37]. In light of our structure, structure-activity relationship (SAR) analysis could be utilized to design even more potent inhibitors that bind to this critical chaperone-usher interface. Furthermore, our structure potentially provides a template for the design of novel small molecules that sterically block the NTD-CTD2 interface to selectively hinder the usher from acting as an assembly platform for the development of antibiotic-sparing therapeutics. In summary, the PapC-PapDG structure and analysis of its activity *in vitro,* provides an extraordinary view of a bacterial nanomachine caught in the act of being primed to catalyze macromolecular protein assembly across the outer membrane. Moreover, this structure may facilitate the development of new drugs that block chaperone-adhesin translocation to prevent assembly of one of the bacterium's major virulence factors.

Methods

Expression and purification of the full-length wild-type PapC usher.

Plasmid pDG2 encoding wild-type PapC with a thrombin cleavage site and a 6× HIS tag added to the C-terminus and the multi-porin mutant BL21(DE3)Omp8 *E. coli* strain were used for PapC expression as previously described[38]. For protein expression, *E. coli* was grown at 37 ºC with aeration in LB medium supplemented with 100 μg/mL ampicillin and was induced at an OD_{600} of 0.6–0.8 for 2 hours at 37 ºC by the addition of 0.1% L-arabinose. To isolate the outer membrane (OM) fraction, resuspended cells supplemented with 1× EDTA-free protease inhibitor cocktail (Pierce) and DNAse I were subjected to microfluidizer cell disruption via 4 passes at 30 kPsi. Unbroken cells were removed by centrifugation at 4,500 × g for 10–12 minutes at 4 ºC. Lysed cells were centrifuged at 39,000 × g for 60 minutes at 4 ºC to pellet total membranes. Total membranes were resuspended using a dounce homogenizer and extracted with 1% Sarkosyl by stirring at 25 ºC for 45 minutes. OM was pelleted by centrifugation at 39,000 × g for 60 minutes at 4 ºC and then was solubilized by resuspension using a dounce homogenizer in 20 mM Tris-HCl pH 8.0, 300 mM NaCl, 1× Pierce Protease Inhibitor Cocktail, and 1% dodecyl-maltopyranoside (DDM, Sol-grade; Anatrace) and stirring overnight at 4 ºC. The OM extract was clarified by centrifugation at 39,000 × g for 30 minutes at 4 ºC. The clarified OM extract was added to 3 mL nickel affinity resin equilibrated with 20 mM Tris-HCl pH 8.0, 300 mM NaCl, 0.2% DDM, 20 mM imidazole (Buffer A). OM extract/nickel resin slurry was stirred slowly at 4 ºC for 3 hours to allow batching binding of PapC to nickel affinity resin. Batch bound resin was added to a 30 mL polypropylene column and washed with 10 column volumes (CV) of Buffer A. PapC was eluted with 3 CV 20 mM Tris-HCl pH 8.0, 100 mM NaCl, 0.1% DDM, 400 mM imidazole (Buffer B).

Expression and purification of the PapDG chaperone-adhesin complex.

Plasmids pDF1 (encoding PapD and pTrcGII (encoding PapG) and the *E. coli* C600 strain were used for PapDG expression[21,39]. Periplasm was prepared as described previously[16]. Periplasm was dialyzed into 1× PBS supplemented with 250 mM NaCl (Buffer C) and loaded onto a Cobalt HTC agarose column (Goldbio). PapDG was eluted with a linear gradient of Buffer C with 0–300 mM imidazole where the complex eluted in 210 mM imidazole. Fractions containing PapDG were pooled and dialyzed into 20 mM Tris-HCl pH 8.0, 500 mM $(NH_4)_2SO_4$ (Buffer D) for a second Butyl 4FF column (GE Healthcare). PapDG was eluted with a linear gradient of Buffer D at 250 mM $(NH_4)_2SO_4$. Fractions containing PapDG were pooled for a final Cobalt HTC agarose column (Goldbio). Using a linear gradient of Buffer C with 0–300 mM imidazole, the complex was eluted in 180 mM imidazole. The fractions containing PapDG were dialyzed into 20 mM Tris-HCl pH 8.0, 100 mM NaCl and 0.1% DDM (Sol-grade; Anatrace) for *in vitro* ternary complex reconstitution.

In vitro reconstitution and purification of wild-type and mutant PapC-PapDG.

Affinity purified PapC (ε at 280 nm = 156330 M^{-1} cm^{-1}) and column-purified PapDG (ε at 280 nm = 99615 M^{-1} cm^{-1}) were mixed in a 1:1.2 molar ratio (2.2 μM-6.3 μM: 2.6–7.5 μM) in Buffer B and were allowed to form stable complex by rotating gently at 4 ºC for 1 hour, prior to size-exclusion chromatography (SEC). The mixture was concentrated using a 100 kDa MWCO centrifugal device (Amicon), loaded onto a Superose 6 10/300 GL column (GE Healthcare), and purified at 4 ºC in buffer containing 20 mM Tris-HCl pH 8.0, 50 mM NaCl, and 5 mM 5-cyclohexyl-1-pentyl-β-d-maltoside (CYMAL-5, Anagrade; Anatrace) (Buffer E). The fractions corresponding to PapC-PapDG complex were collected and concentrated using a 100 kDa MWCO centrifugal device (Amicon) for crystallization or DSE experiments.

Donor strand exchange (DSE) assay of wild-type and mutant PapC-PapDG with PapDF.

SEC purified wild-type PapC-PapDG or F745A PapC-PapDG ternary complex (ε at 280 nm = 255945 M^{-1} cm^{-1}) and PapDF (ε at 280 nm = 39100 M^{-1} cm^{-1}) were mixed in a 1:3 molar ratio (4 μM:12 μM) in Buffer E and allowed to undergo DSE at 25 ºC. Reactions were conducted using identical protein concentrations and reaction volumes. Samples were taken over a 48-hour time course and quenched with SDS loading buffer and stored at −20 ºC. Unboiled samples were analyzed by 12% SDS-PAGE to monitor the formation of a PapG-PapF interaction over time. Bio-Rad Image Lab™ was used to analyze and quantify PapG-PapF band at t = 48 hours for mutant PapC-PapDG sample relative to wild-type PapC-PapDG sample. Subunit-subunit interactions are SDS-resistant when left unboiled at room temperature while chaperone-subunit interactions are not. Therefore, the formation of a stable PapG-PapF band is indicative of a productive subunit-subunit interaction and of a PapC usher capable of promoting DSE *in vitro*.

Purification of wild-type PapC-PapDFG.

Sample subjected to the DSE assay was concentrated using a 100 kDa MWCO centrifugal device (Amicon), loaded onto a Superose 6 10/300 GL column (GE Healthcare), and purified at 4 ºC in Buffer E. Fractions corresponding to the PapC-PapDFG complex were

individually collected and concentrated 5-fold using a 100 kDa MWCO centrifugal device (Amicon), and analyzed by 12% SDS-PAGE.

Crystallization and structure determination of PapC-PapDG.

Crystals of the PapC-PapDG ternary complex were grown using sitting-drop vapor diffusion by mixing 0.3 μL protein with 0.3 μL reservoir solution and incubating at 20 ºC. The crystallization drops contained 9–11 mg/mL (58.4–71.4 μM) of purified complex (ε at 280 nm = 255945 M^{-1} cm^{-1}), 50 mM sodium citrate pH 5.0–6.0, 50 mM lithium sulfate, 50 mM sodium sulfate and 7–14% PEG 4000. Crystals of two distinct morphologies appeared in the same drops, only plate-like crystals diffracted X-rays beyond 4 Å resolution. Crystals appeared in one week and grew to full size within two weeks. Plate-like crystals were flash-cooled in liquid nitrogen using the mother liquor supplemented with 5 mM CYMAL-5 and 30% (v/v) glycerol as cryoprotectant.

Diffraction data were collected at the Advanced Photon Source beamline 24-ID-E and were integrated and scaled using the HKL2000 package[40]. Because of strong anisotropy the dataset was corrected using the UCLA-DOE Diffraction Anisotropy server[41]. After truncation the resolution limit along the reciprocal cell directions a*, b*, and c* was 3.7, 4.6 and 3.7 Å, respectively. An isotropic B-factor of −47.12 $Å^2$ was applied to restore the magnitude of high-resolution reflections. The crystal belonged to space group $C222_1$ with one PapC-PapDG complex per asymmetric unit.

Phasing was obtained by molecular replacement using Phaser with structures of the PapC translocation domain (PDB ID: 2VQI), PapD-PapG pilin domain (PDB ID: 2WMP), PapG lectin domain (PDB ID: 1J8S) and PapC CTD2 domain (PDB ID: 3L48) as search models[42]. Cycles of model building and refinement were carried out in Coot and REFMAC before building the remaining of the complex[43,44]. For model building of the PapC NTD and CTD1, the PapC NTD and CTD1 models were first generated based on the full-length FimD structure (PDB ID: 3RFZ) using the SWISS-MODEL server[45]. The NTD model was fitted into the electron density using rigid body fit in Coot and was then manually adjusted. The PapC NTD tail (residues 1–30) and the linker between the PapC NTD and the translocation domain were manually built. At the CTD1 location there was clear electron density corresponding to three β-strands, one of which connects to CTD2. Based on this observation, the CTD1 model was placed into the electron density and was then manually adjusted. The assignment of the sequence register for the PapC NTD and CTD1 was based on the model generated from SWISS-MODEL. The complete model was iteratively adjusted and refined. At the final refinement step the TLS and “jelly body” refinement were applied when running REFMAC. The final model, refined to R_{work}/R_{free} = 0.282/0.329, contains: PapC residues 1–54, 67–248, 252–347, 355–430, 435–588, 592–633, 651–662, 672–687, 714–808; PapD residues 1–215; PapG residues 1–316. Residues without sidechain density were modeled as alanine. Percentage of residues in favored, allowed and disallowed regions of the Ramachandran plot were 92%, 8%, and 0%, respectively[47].

Calculation of domain movements using DynDom

Domain movements between the pre-activation and post-activation usher states were calculated using the DynDom Protein Domain Motion Analysis web server[46]. DynDom requires the use of two different conformations of the same protein or protein complex. In order to create a post-activation PapC-PapDG usher model, the individual TD, NTD, and CTD2 domains were superimposed to the corresponding domains in the FimD-FimCH structure (PDB ID: 3RFZ) and each resulting superimposed domain was exported as a molecule. Merging the coordinates of TD and NTD or TD and CTD2 created models of the post-activation TD-NTD and TD-CTD2 structures, where the TD was used as the static domain and the NTD or CTD2 were considered dynamic domains. To create an equivalent model in the pre-activation usher state, TD-NTD or TD-CTD2 were exported as molecules from our solved structure. Pre-activation TD-NTD or TD-CTD2 and post-activation TD-NTD or TD-CTD2 molecules were input as conformer 1 and conformer 2, respectively. The resulting output reported the translation and rotation for the dynamic domain in question, which are described in the figure legends.

Functional analysis of PapC mutants

All PapC mutants were derived from plasmid pDG2 using site-directed mutagenesis[38]. We created the following mutations: i) substitution of residues 12–21 to alanine (12–21A); ii) substitution of residues 16–20 to alanine (16–20A); iii) introduction of a proline residue at position 17 (D17P) and position 19 (T19P) to specifically disrupt the beginning and middle of the NTD N-terminal α-helix; and iv) substitution of alanine for a conserved phenylalanine (F745A) in CTD2. All constructs generated with site-directed mutagenesis methods were sequenced to verify that the correct mutations were made. The HA titer of C600 cells harboring pEV33[47], a Tetracycline (Tet)-resistant, tryptic soy agar (TSA)-inducible plasmid containing the entire *pap* operon with PapC inactivated by a XhoI linker, and each *papC* mutant plasmid was determined by overnight growth on selective TSA media supplemented with 100 μg/mL ampicillin, 15 μg/mL tetracycline, and 0.005% L-arabinose. HA titer assays were performed as previously described[48]. The HA endpoint was defined as the last dilution well before erythrocyte buttons formed. Titers are represented as the reciprocal of the endpoint dilution. The statistical significance of differences between wild-type and mutant PapC in experiments was determined by an unpaired two-tailed Mann–Whitney test. Statistical analyses were performed using Graphpad Prism 7.

Data availability

The data that support the findings of this study are available from the corresponding authors upon request. Atomic coordinates and structure factors for the reported crystal structure have been deposited into the Protein Data Bank (PDB) under accession code 6CD2.

Code availability

No new code was generated for this study. All software was obtained from publicly available sources; papers describing the software are cited in the text.

Statistical analysis

No statistical methods were used to predetermine sample size. The statistical significance of differences between samples in experiments was determined by an unpaired two-tailed Mann–Whitney test. Statistical analyses were performed using Graphpad Prism 7.

Supplementary Material

Refer to Web version on PubMed Central for supplementary material.

Acknowledgements

We thank the staff of beamline 24-ID-E at APS, especially K. Rajashankar, K. Perry, and N. Sukumar for assistance. This work used NE-CAT beamlines (GM103403), a Pilatus detector (RR029205), an Eiger detector (OD021527) at the APS (DE-AC02–06CH11357). This work was supported by grants from the NIH (R01AI029549 (S.J.H), R01AI048689 (S.J.H)), and the National Science Foundation (DGE-1745038 (N.S.O.)), and start-up funds from Washington University School of Medicine (P.Y.).

References

1. Nuccio SP & Baumler AJ Evolution of the chaperone/usher assembly pathway: fimbrial classification goes Greek. Microbiol Mol Biol Rev 71, 551–575, doi:10.1128/MMBR.00014-07 (2007). [PubMed: 18063717]
2. Ford B et al. Structural homology between the C-terminal domain of the PapC usher and its plug. J Bacteriol 192, 1824–1831, doi:10.1128/JB.01677-09 (2010). [PubMed: 20118254]
3. Nishiyama M et al. Structural basis of chaperone-subunit complex recognition by the type 1 pilus assembly platform FimD. EMBO J 24, 2075–2086, doi:10.1038/sj.emboj.7600693 (2005). [PubMed: 15920478]
4. Phan G et al. Crystal structure of the FimD usher bound to its cognate FimC-FimH substrate. Nature 474, 49–53, doi:10.1038/nature10109 (2011). [PubMed: 21637253]
5. Remaut H et al. Fiber formation across the bacterial outer membrane by the chaperone/usher pathway. Cell 133, 640–652, doi:10.1016/j.cell.2008.03.033 (2008). [PubMed: 18485872]
6. Thanassi DG, Stathopoulos C, Dodson K, Geiger D & Hultgren SJ Bacterial outer membrane ushers contain distinct targeting and assembly domains for pilus biogenesis. J Bacteriol 184, 6260–6269 (2002). [PubMed: 12399496]
7. Foxman B Epidemiology of urinary tract infections: incidence, morbidity, and economic costs. Am J Med 113 Suppl 1A, 5S–13S (2002).
8. Foxman B Epidemiology of urinary tract infections: incidence, morbidity, and economic costs. Dis Mon 49, 53–70, doi:10.1067/mda.2003.7 (2003). [PubMed: 12601337]
9. Wurpel DJ, Beatson SA, Totsika M, Petty NK & Schembri MA Chaperone-usher fimbriae of Escherichia coli. PLoS One 8, e52835, doi:10.1371/journal.pone.0052835 (2013). [PubMed: 23382825]
10. Ronald A The etiology of urinary tract infection: traditional and emerging pathogens. Dis Mon 49, 71–82, doi:10.1067/mda.2003.8 (2003). [PubMed: 12601338]
11. Ronald AR et al. Urinary tract infection in adults: research priorities and strategies. Int J Antimicrob Agents 17, 343–348 (2001). [PubMed: 11295419]
12. Melican K et al. Uropathogenic Escherichia coli P and Type 1 fimbriae act in synergy in a living host to facilitate renal colonization leading to nephron obstruction. PLoS Pathog 7, e1001298, doi: 10.1371/journal.ppat.1001298 (2011). [PubMed: 21383970]
13. Roberts JA et al. The Gal(alpha 1–4)Gal-specific tip adhesin of Escherichia coli P-fimbriae is needed for pyelonephritis to occur in the normal urinary tract. Proc Natl Acad Sci U S A 91, 11889–11893 (1994). [PubMed: 7991552]

14. Abraham SN, Sun D, Dale JB & Beachey EH Conservation of the D-mannose-adhesion protein among type 1 fimbriated members of the family Enterobacteriaceae. Nature 336, 682–684, doi: 10.1038/336682a0 (1988). [PubMed: 2904657]
15. Lindberg F, Tennent JM, Hultgren SJ, Lund B & Normark S PapD, a periplasmic transport protein in P-pilus biogenesis. J Bacteriol 171, 6052–6058 (1989). [PubMed: 2572580]
16. Hultgren SJ et al. The PapG adhesin of uropathogenic Escherichia coli contains separate regions for receptor binding and for the incorporation into the pilus. Proc Natl Acad Sci U S A 86, 4357–4361 (1989). [PubMed: 2567514]
17. Choudhury D et al. X-ray structure of the FimC-FimH chaperone-adhesin complex from uropathogenic Escherichia coli. Science 285, 1061–1066 (1999). [PubMed: 10446051]
18. Sauer FG et al. Structural basis of chaperone function and pilus biogenesis. Science 285, 1058–1061 (1999). [PubMed: 10446050]
19. Zavialov AV et al. Structure and biogenesis of the capsular F1 antigen from Yersinia pestis: preserved folding energy drives fiber formation. Cell 113, 587–596 (2003). [PubMed: 12787500]
20. Remaut H et al. Donor-strand exchange in chaperone-assisted pilus assembly proceeds through a concerted beta strand displacement mechanism. Molecular cell 22, 831–842, doi:10.1016/j.molcel.2006.05.033 (2006). [PubMed: 16793551]
21. Sauer FG, Pinkner JS, Waksman G & Hultgren SJ Chaperone priming of pilus subunits facilitates a topological transition that drives fiber formation. Cell 111, 543–551 (2002). [PubMed: 12437927]
22. Geibel S, Procko E, Hultgren SJ, Baker D & Waksman G Structural and energetic basis of folded-protein transport by the FimD usher. Nature 496, 243–246, doi:10.1038/nature12007 (2013). [PubMed: 23579681]
23. Volkan E et al. Domain activities of PapC usher reveal the mechanism of action of an Escherichia coli molecular machine. Proc Natl Acad Sci U S A 109, 9563–9568, doi:10.1073/pnas.1207085109 (2012). [PubMed: 22645361]
24. Baga M, Norgren M & Normark S Biogenesis of E. coli Pap pili: papH, a minor pilin subunit involved in cell anchoring and length modulation. Cell 49, 241–251 (1987). [PubMed: 2882856]
25. Verger D, Miller E, Remaut H, Waksman G & Hultgren S Molecular mechanism of P pilus termination in uropathogenic Escherichia coli. EMBO reports 7, 1228–1232, doi:10.1038/sj.embor.7400833 (2006). [PubMed: 17082819]
26. Nishiyama M, Ishikawa T, Rechsteiner H & Glockshuber R Reconstitution of pilus assembly reveals a bacterial outer membrane catalyst. Science 320, 376–379, doi:10.1126/science.1154994 (2008). [PubMed: 18369105]
27. Saulino ET, Thanassi DG, Pinkner JS & Hultgren SJ Ramifications of kinetic partitioning on usher-mediated pilus biogenesis. EMBO J 17, 2177–2185, doi:10.1093/emboj/17.8.2177 (1998). [PubMed: 9545231]
28. Li Q et al. The differential affinity of the usher for chaperone-subunit complexes is required for assembly of complete pili. Mol Microbiol 76, 159–172, doi:10.1111/j.1365-2958.2010.07089.x (2010). [PubMed: 20199591]
29. Jacob-Dubuisson F, Heuser J, Dodson K, Normark S & Hultgren S Initiation of assembly and association of the structural elements of a bacterial pilus depend on two specialized tip proteins. EMBO J 12, 837–847 (1993). [PubMed: 8096174]
30. Lee YM, Dodson KW & Hultgren SJ Adaptor function of PapF depends on donor strand exchange in P-pilus biogenesis of Escherichia coli. J Bacteriol 189, 5276–5283, doi:10.1128/JB.01648-06 (2007). [PubMed: 17496084]
31. Rose RJ et al. Unraveling the molecular basis of subunit specificity in P pilus assembly by mass spectrometry. Proc Natl Acad Sci U S A 105, 12873–12878 (2008). [PubMed: 18728178]
32. Verger D et al. Structural determinants of polymerization reactivity of the P pilus adaptor subunit PapF. Structure 16, 1724–1731, doi:10.1016/j.str.2008.08.012 (2008). [PubMed: 19000824]
33. Eidam O, Dworkowski FS, Glockshuber R, Grutter MG & Capitani G Crystal structure of the ternary FimC-FimF(t)-FimD(N) complex indicates conserved pilus chaperone-subunit complex recognition by the usher FimD. FEBS letters 582, 651–655 (2008). [PubMed: 18242189]
34. Nishiyama M et al. Structural basis of chaperone-subunit complex recognition by the type 1 pilus assembly platform FimD. The EMBO Journal 24, 2075–2086 (2005). [PubMed: 15920478]

35. Ng TW, Akman L, Osisami M & Thanassi DG The usher N terminus is the initial targeting site for chaperone-subunit complexes and participates in subsequent pilus biogenesis events. J Bacteriol 186, 5321–5331, doi:10.1128/JB.186.16.5321-5331.2004 (2004). [PubMed: 15292133]

36. Werneburg GT et al. The pilus usher controls protein interactions via domain masking and is functional as an oligomer. Nat Struct Mol Biol 22, 540–546, doi:10.1038/nsmb.3044 (2015). [PubMed: 26052892]

37. Pinkner JS et al. Rationally designed small compounds inhibit pilus biogenesis in uropathogenic bacteria. Proc Natl Acad Sci U S A 103, 17897–17902, doi:10.1073/pnas.0606795103 (2006). [PubMed: 17098869]

38. Henderson NS & Thanassi DG Purification of the outer membrane usher protein and periplasmic chaperone-subunit complexes from the P and type 1 pilus systems. Methods Mol Biol 966, 37–52, doi:10.1007/978-1-62703-245-2_3 (2013). [PubMed: 23299727]

39. Dodson KW et al. Structural basis of the interaction of the pyelonephritic E. coli adhesin to its human kidney receptor. Cell 105, 733–743 (2001). [PubMed: 11440716]

40. Otwinowski Z & Minor W Processing of X-ray diffraction data collected in oscillation mode. Methods Enzymol 276, 307–326 (1997).

41. Strong M et al. Toward the structural genomics of complexes: crystal structure of a PE/PPE protein complex from Mycobacterium tuberculosis. Proc Natl Acad Sci U S A 103, 8060–8065, doi:10.1073/pnas.0602606103 (2006). [PubMed: 16690741]

42. McCoy AJ et al. Phaser crystallographic software. J Appl Crystallogr 40, 658–674, doi:10.1107/S0021889807021206 (2007). [PubMed: 19461840]

43. Emsley P & Cowtan K Coot: model-building tools for molecular graphics. Acta Crystallogr D Biol Crystallogr 60, 2126–2132, doi:10.1107/S0907444904019158 (2004). [PubMed: 15572765]

44. Murshudov GN, Vagin AA & Dodson EJ Refinement of macromolecular structures by the maximum-likelihood method. Acta Crystallogr D Biol Crystallogr 53, 240–255, doi:10.1107/S0907444996012255 (1997). [PubMed: 15299926]

45. Arnold K, Bordoli L, Kopp J & Schwede T The SWISS-MODEL workspace: a web-based environment for protein structure homology modelling. Bioinformatics 22, 195–201, doi:10.1093/bioinformatics/bti770 (2006). [PubMed: 16301204]

46. Hayward S & Berendsen HJ Systematic analysis of domain motions in proteins from conformational change: new results on citrate synthase and T4 lysozyme. Proteins 30, 144–154 (1998). [PubMed: 9489922]

47. Volkan E et al. Molecular basis of usher pore gating in Escherichia coli pilus biogenesis. Proc Natl Acad Sci U S A 110, 20741–20746, doi:10.1073/pnas.1320528110 (2013). [PubMed: 24297893]

48. Slonim LN, Pinkner JS, Branden CI & Hultgren SJ Interactive surface in the PapD chaperone cleft is conserved in pilus chaperone superfamily and essential in subunit recognition and assembly. EMBO J 11, 4747–4756 (1992). [PubMed: 1361168]

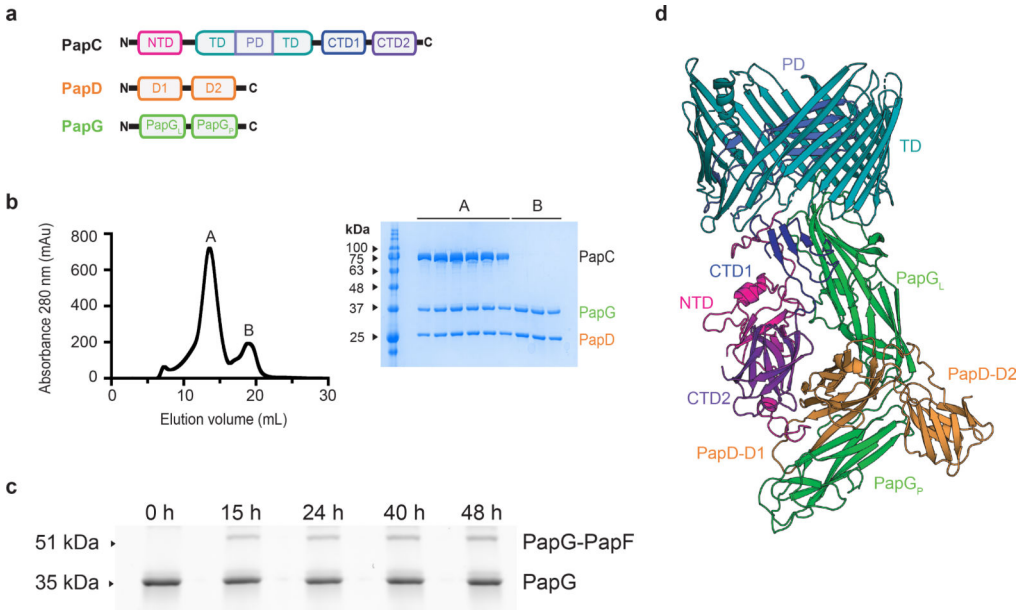

Figure 1 |. Structure of the PapC-PapDG ternary complex.

a, Schematic diagram of domain organization of PapC, PapD (PapD-D1, N-terminal domain PapD-D2, C-terminal domain), and PapG ($PapG_L$, lectin domain $PapG_P$, pilin domain). **b**, *In vitro* reconstitution of PapC-PapDG yields stable ternary complex indicated by size-exclusion chromatography. SDS-PAGE shows that Peak A represents the PapC-PapDG ternary complex and Peak B represents excess PapDG. **c,** Donor-strand exchange (DSE) assay demonstrating that the purified PapC-PapDG complex is functional. PapC-PapDG was challenged at t= 0 with PapDF. SDS-PAGE visualized formation of PapG-PapF intermediate at each collected time point (See Methods for detail). n=3 replicates. **d**, Overall architecture of the PapC-PapDG ternary complex. Domains are distinctly colored.

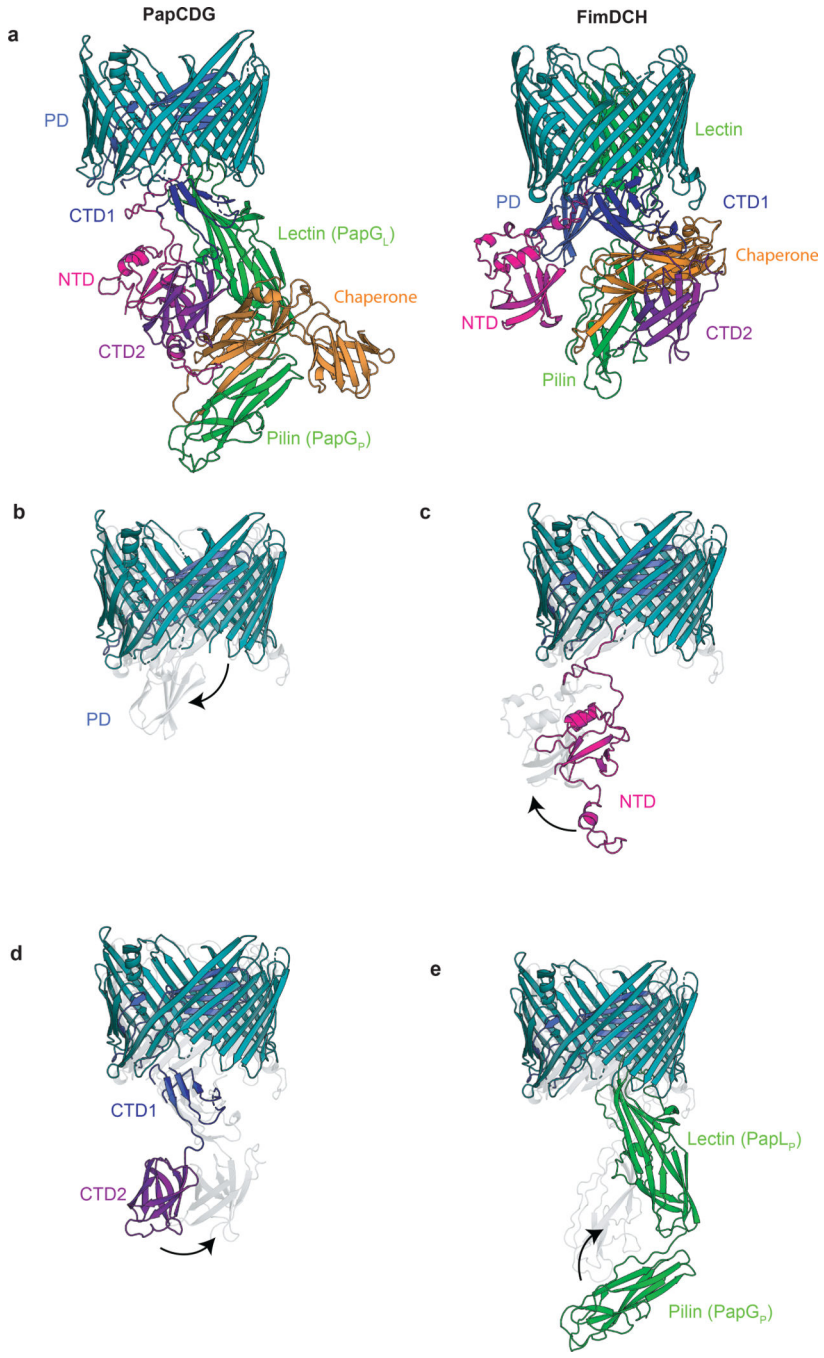

Figure 2 |. Comparison of the pre-activation PapC-PapDG and the post-activation FimD-FimCH structures.

a, Side-view of PapC-PapDG and FimD-FimCH (PDB ID: 3RFZ) structures. The chaperones (PapD and FimC), adhesins (PapG and FimH) and ushers (PapC and FimD) are colored identically. **b-e**, Domain movements required for transition from the pre-activation (PapC-PapDG) usher state to the post-activation (FimD-FimCH) usher state (PDB ID: 3RFZ). FimD-FimCH is depicted in grey. Domain movements between the two conformational states were calculated using the DynDom protein domain analysis server[31].

The reported translation/rotation values for the dynamic domains were the following: (**b**) PD (20 Å / 114°); (**c**) NTD (13 Å / 47°), (**d**) CTD2 (19 Å / 87°) and (**e**) $PapG_P$ (19 Å / 87°).

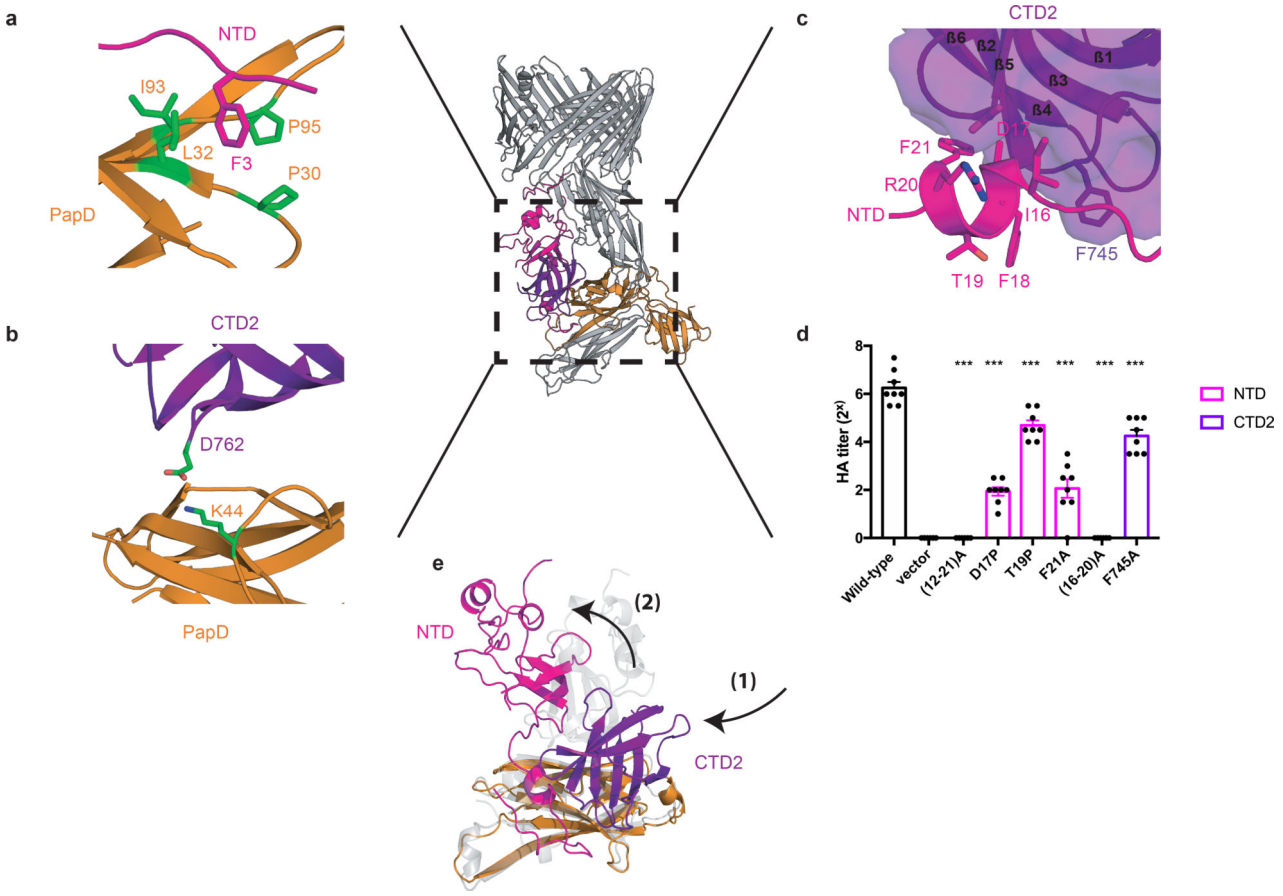

Figure 3 |. Tripartite interface between PapD and the NTD and CTD2 of PapC.

a, NTD-PapD interface. F3 of the PapC NTD interacts with a hydrophobic pocket comprised of P30, L32, I93, P95 of the PapD chaperone. Chaperone residues are colored green for clarity. **b**, CTD2-PapD interface. A salt bridge is formed between K44 of PapD and D762 of PapC CTD2. Side chains are colored by atom types. **c**, NTD-CTD2 interface. Residues that play an important role at this interface, as measured by hemagglutination titer analysis (**d**) are highlighted. **d**, Hemagglutination assays were performed to test the ability of PapC mutants to complement a Δ*papC pap* operon (*papAHDJKEFG*) for assembly of adhesive P pili on the bacterial surface. The HA titer represents the highest fold dilution of bacteria capable of agglutinating human red blood cells. Titers are represented as the reciprocal of the endpoint dilution. Data are represented as mean ± s.e.m. Statistical analyses were performed using unpaired two-tailed Mann-Whitney test; ***P= 0.0002 and ***P=0.0009 (T19P PapC). n= 8 replicates. Replicates are biological. **e**, Proposed mechanism of subunit transfer from NTD to CTD2. Superposition of PapC-PapDG with FimD NTD-FimC-$FimH_P$ (PDB ID: 1ZE3) demonstrates that CTD2 would directly clash with the NTD as it interacts with chaperone-adhesin during the initial targeting step. Subunit transfer may occur when CTD2 reaches over to interact with the N-terminal tail and chaperone **(1)**, which results in displacement of the NTD from the main interaction interface **(2)**.

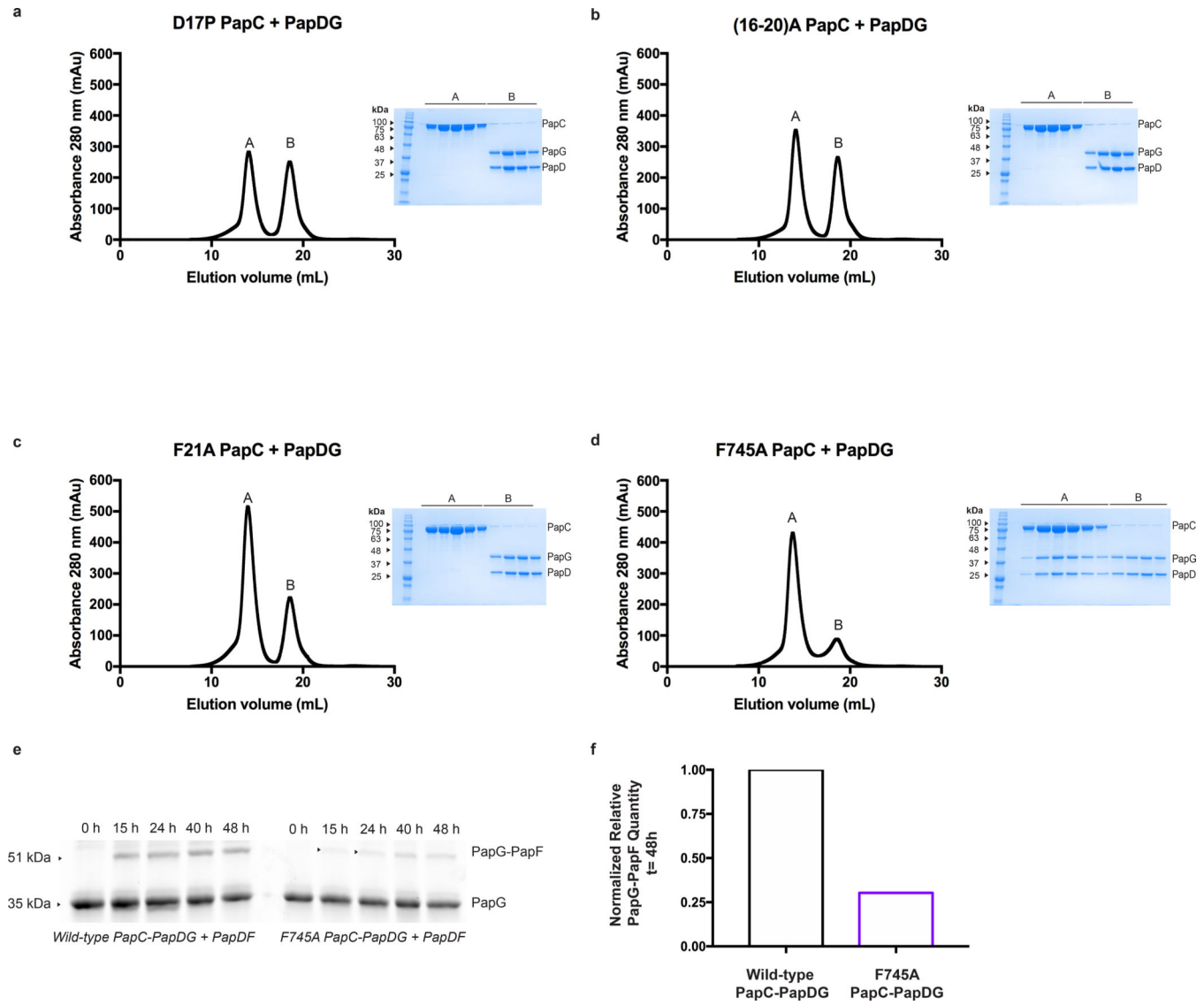

Figure 4 |. PapC NTD and CTD2 mutants are defective for usher activation.

a-c, *In vitro* reconstitution of NTD mutated PapC-PapDG does not yield stable ternary complex indicated by size-exclusion chromatography. SDS-PAGE shows that Peak A represents the mutant PapC alone and Peak B represents excess PapDG. n=1 replicate. **d**, *In vitro* reconstitution of CTD2 mutated PapC-PapDG yields stable ternary complex indicated by size-exclusion chromatography. SDS-PAGE shows that Peak A represents the mutant PapC-PapDG ternary complex and Peak B represents excess PapDG. n=1 replicate. **e**, Donor-strand exchange (DSE) assay demonstrates F745A PapC-PapDG is less efficient at promoting DSE at each time point compared to wild-type PapC-PapDG (**Fig. 1c**). F745A PapC-PapDG was challenged at t= 0 with PapDF. SDS-PAGE analysis visualized formation of PapG-PapF intermediate at each collected time point. **f**, Quantification of PapG-PapF band at t= 48 h demonstrates reduction in F745A PapC-PapDG mediated DSE relative to wild-type PapC-PapDG.